

Aerial Grasping based on Shape Adaptive Transformation by HALO: Horizontal Plane Transformable Aerial Robot with Closed-loop Multilinks Structure

Tomoki Anzai¹, Moju Zhao¹, Shunichi Nozawa¹, Fan Shi¹, Kei Okada¹, Masayuki Inaba¹

Abstract—In this paper, we present the achievement of aerial grasping by shape adaptive transformation to the object shape, using a novel transformable aerial robot called HALO: Horizontal Plane Transformable Aerial Robot with Closed-loop Multilinks Structure. Aerial manipulation is an active research area and using multiple aerial robots is an effective solution for the large size object. However the cooperation is considered that there are some difficulties such as the synchronized flight control and collision with each other. Then, we focus on the transformable aerial robot with two-dimensional multilinks proposed in our previous works, which can transform to the suitable form for the target object and grasp it. However the transformable aerial robot with the serial-link structure could not achieve stable flight in terms of horizontal position and yaw control due to the low rigidity and large inertia in the case of more than 4 links. Thus, first we construct a novel type of multilinks with closed-loop structure to avoid the deformation and a new link module with a tilted propeller for fully-actuated control. Second, we describe transformation method with closed-loop multilinks. Third, we present the optimization planning method for the multilinks form to be adaptive to the two-dimensional shape of the target object. Finally, we present experimental results to demonstrate the feasibility of closed-loop aerial transformation and aerial grasping for the large size object.

I. INTRODUCTION

Nowadays, aerial robots are studied actively. Due to their high mobility in three-dimensional space, aerial manipulation and transportation have attracted a lot of attention[1][2][3][4][5] and cooperative aerial manipulation has become an active research area[6][7][8][9]. Fink et al.[6] proposed an aerial manipulation system in which three quadrotors cooperate and transport a triangle object tracking the desired trajectory. One of the advantages of using multiple aerial robots for aerial manipulation is that we can address the object 2D shape easily during the manipulation and transportation. On the other hand, there are also some challenges to use multiple aerial robots, such as the decentralized communication and synchronized flight control. The decentralized communication depends on environments, so it is difficult to construct a reliable multi-robot system. Furthermore, the collision among aerial robots is another significant problem. To avoid the collision, we must consider a constraint that aerial robots should keep enough distance from each other. Based on the above, a single aerial robot

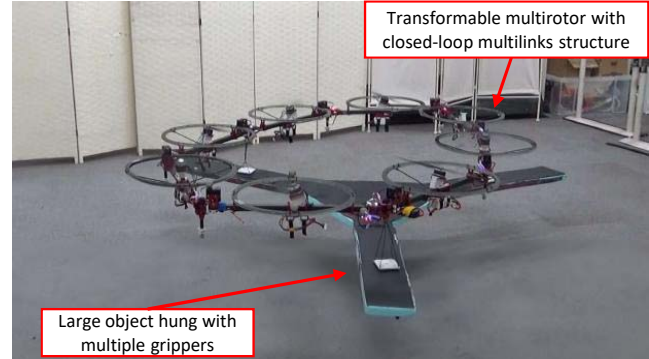


Fig. 1. Shape adaptive grasping by octocopter with closed-loop multilinks structure.

is also an alternative solution to manipulate objects[10]. In case of using a single aerial robot, there is no concern for interruption of communication and collision, but the lower flexibility for shape of objects compared to cooperative aerial manipulation.

Then, to achieve grasping with various shapes by a single aerial robot, we focus on multirotor with two-dimensional multilinks[11][12][13] which is capable of transforming in the air. We propose a system in which the multirotor with multilinks transforms to an adaptive form to the 2D shape of the target object and grasps it using gripper hung by cables(Fig. 1). The advantage of this method is that the single multirotor can grasp large size object with various shapes, but the drawback is that low flight endurance due to its larger weight compared to multi-robot system. In our previous research[13], we achieved the hardware platform of the multilinks, but in the experiment the hex type robot with serial link structure could not fly stably in terms of yaw control due to the lack of rigidity of link module. Although constructing more rigid link module is one of the solutions, there is a trade-off between the rigidity and the weight. There was also a problem that the trackability of horizontal position(x, y) was low due to the large inertia of the body. Therefore, in this paper, we propose a new type of multilinks with closed-loop structure to avoid the deformation resulting from the low rigidity. Moreover, to improve the position trackability, we use fully-actuated control[14] instead of conventional under-actuated control with tilted propellers. Since the closed-loop structure has the geometric constraint, leading to the low degree of freedom to transform compared

¹T. Anzai, M. Zhao, S. Nozawa, F. Shi, K. Okada and M. Inaba are with Department of Mechano-Informatics, The University of Tokyo, 7-3-1 Hongo, Bunkyo-Ku, Tokyo 113-8656, Japan anzai at jsk.t.u-tokyo.ac.jp

to the open-loop structure, we develop octo type with eight links which has five degree of freedom of transformation. We name this robot HALO(Horizontal Plane Transformable Aerial Robot with Closed-Loop Multilinks Structure.)

The main purpose of this paper is to achieve the aerial grasping by the adaptive transformation to the object 2D shape using HALO. In Sec. II, we introduce the construction of link module along with the fully-actuated flight control. In Sec. III, we describe transformation method with two-dimensional closed-loop structure. Sec. IV explains how to obtain the optimal form of the multilinks for the target object. Finally, we present experimental results in Sec. V to show the feasibility of the closed-loop aerial transformation and corresponding grasping for large size objects with various 2D shapes.

II. TRANSFORMABLE AERIAL ROBOT PLATFORM

A. Structure of Link Module

In our previous work[13], we constructed a hardware platform of the multirotor with multilinks. Fig. 2 shows the octorotor with closed-loop multilinks(a) and the link module(b). Each link module has a built-in propeller at the center, a servo motor at the end and a controller board which controls the motor and servo motor. The rotation range of each joint is $-\frac{\pi}{2} \sim \frac{\pi}{2}$ rad. The multilinks can transform only in two-dimensions due to the joints with the parallel rotational axis. The range of thrust is $0 \sim 16.5$ N. The length of each link is 0.6 m while the diameter of the propeller protector is 0.38 m. The payload is about 5 kg. While our previous multirotor[12][13] had parallel propellers, the multirotor of this work has tilted propellers to achieve a fully-actuated control. There are two types of link as shown in Fig. 2(c-1) and (c-2). The tilt angle from vertical is 20° , and the direction is opposite between (c-1) and (c-2). This tilt angle is chosen for initial test with reference to [15]. Furthermore, the propeller rotation directions (CW and CCW) are also opposite to cancel the counter torques. The two types of link are connected alternately as shown in Fig. 2(a).

B. Flight Control

For conventional aerial robots, under-actuated control is general. Recently, fully-actuated control[14][16] has become an alternative control method. The advantage of under-actuated system is that at least only four propellers are required and the flight efficiency is high because all the propeller directions are vertical to the ground. On the other hand, the advantage of fully-actuated control is that the application is widely ranging because the position and orientation can be controlled independently: however, the drawback is that at least six propellers are required and the flight efficiency is low due to the tilted propellers. With regard to our transformable aerial robot, the inertia is larger than conventional aerial robots because heavy parts such as battery, joint servo motor and carbon frame are located apart from the CoG. In the under-actuated control, the horizontal position(x, y) is controlled by tilting the whole body around

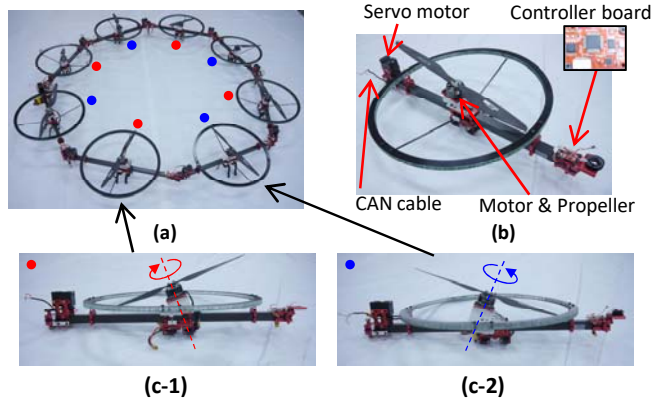


Fig. 2. Transformable aerial robot platform. (a): octorotor with closed-loop link structure consisting of the link modules. The red and blue points indicate the type of links shown in (c-1) and (c-2). (b): link module which has a built-in propeller at the center, a servo motor at the end and a controller board which controls the motor and servo motor. (c-1), (c-2): two types of link module which have opposite thrust directions and opposite propeller rotation directions (CW and CCW).

X and Y axis, but the responsiveness of tilt is low due to the large inertia. Therefore, we apply fully-actuated control to the transformable multirotor.

1) *Dynamic Model:* We assume that the multilinks act as a single rigid body at each time point with mass M and inertia \mathbf{I} . In other words, the aerial transformation is operated slowly. While M is constant, \mathbf{I} changes by transformation. With this assumption, the dynamics of the translational and rotational motion are given as

$$M\ddot{\mathbf{r}} = \mathbf{R}\mathbf{f} - Mg; \mathbf{R} = \mathbf{R}_z(\psi)\mathbf{R}_y(\theta)\mathbf{R}_x(\varphi) \quad (1)$$

$$\mathbf{I}\dot{\boldsymbol{\omega}} = \boldsymbol{\tau} - \boldsymbol{\omega} \times \mathbf{I}\boldsymbol{\omega} \quad (2)$$

where \mathbf{r} is the CoG position and $\boldsymbol{\omega}$ is the vector of the angular velocity of the multilinks. $[\varphi \theta \psi]$ is Euler angles roll, pitch and yaw. Then, \mathbf{f} and $\boldsymbol{\tau}$ are the force and torque acting on the CoG respectively. They are generated by all propeller thrusts $\mathbf{u} = [u_1 \dots u_N]$ and this relationship can be written as follows:

$$\mathbf{f} = \sum_{i=1}^N u_i \mathbf{x}_i \quad (3)$$

$$\boldsymbol{\tau} = \sum_{i=1}^N u_i (\mathbf{p}_i \times \mathbf{x}_i) \quad (4)$$

where \mathbf{x}_i is a unit vector which denotes the rotor direction, and \mathbf{p}_i is the rotor position from CoG respectively. In this work, since we assume that the counter torques are canceled and the influence to the dynamics is sufficiently small, we neglect the counter torques. Eq. 3 and Eq. 4 can be integrated into a simultaneous equation as

$$\begin{bmatrix} \mathbf{f} \\ \boldsymbol{\tau} \end{bmatrix} = \mathbf{Q}\mathbf{u}; \mathbf{Q} = \begin{bmatrix} \mathbf{p}_1 & \mathbf{p}_2 & \cdots & \mathbf{p}_N \\ \mathbf{p}_1 \times \mathbf{x}_1 & \mathbf{p}_2 \times \mathbf{x}_2 & \cdots & \mathbf{p}_N \times \mathbf{x}_N \end{bmatrix} \quad (5)$$

2) *Control:* We use simple PID controller for position and attitude control. The desired force and torque are calculated by Eq. 6 and Eq. 7.

$$\mathbf{f}_{des} = M\mathbf{R}^{-1}(K_{f,p}\mathbf{r}_{err} + K_{f,i} \int \mathbf{r}_{err} + K_{f,d}\dot{\mathbf{r}}_{err}) \quad (6)$$

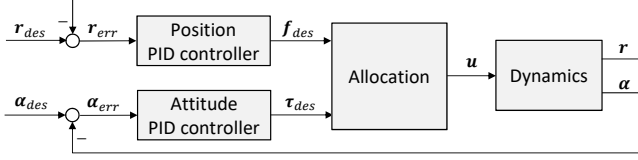


Fig. 3. Flight control system of the multirotor. The input is three-dimensional position $[r_x \ r_y \ r_z]$ and attitude $[\varphi \ \theta \ \psi]$. PID controllers calculate desired force f_{des} and torque τ_{des} , and they are allocated to each propeller thrust u .

$$\begin{aligned} \tau_{des} = \mathbf{I}(K_{\tau,p}\alpha_{err} + K_{\tau,i} \int \alpha_{err} + K_{\tau,d}\dot{\alpha}_{err}) \\ + \boldsymbol{\omega} \times \mathbf{I}\boldsymbol{\omega}; \\ \boldsymbol{\alpha} = [\varphi \ \theta \ \psi] \end{aligned} \quad (7)$$

where r_{err} is the position error and α_{err} is the attitude angles error, respectively. Next, we decompose the desired force f_{des} and torque τ_{des} to each propeller thrust u . The relationship is described in Eq. 5. If $N = 6$ and Q is full rank, Eq. 5 can be solved as $u = Q^{-1}[f^T \ \tau^T]^T$. However, we address octocopter($N=8$) in this work, resulting in an infinite solution for u . Therefore, we choose the pseudo-inverse which minimizes the norm of u . This is given by

$$Q^\# = Q^T(QQ^T)^{-1} \quad (8)$$

Then the propeller thrusts are calculated as

$$u = Q^\# \begin{bmatrix} f_{des} \\ \tau_{des} \end{bmatrix} \quad (9)$$

Note that matrix Q is not constant for the transformable multirotor, so when the form of the multirotor changes, we must update Q and $Q^\#$ for the flight control. Moreover, Q is not always full rank, so that we must avoid such cases. This will be described in the next section. The flow diagram of the whole flight control system is shown in Fig. 3.

III. AERIAL TRANSFORMATION WITH CLOED-LOOP MULTILINKS

In this section, we describe transformation method with two-dimensional closed-loop multilinks. The parallel manipulator[17][18] which has closed-loop structure is so famous and often used in industry. The main interest of the parallel manipulator is the operation of the pose of end effector. However, our interest is the form of the multilinks, in other words, the joint angles. In our previous works[12][13], we simply sent the target angles to the joint angles controller and achieved the aerial transformation. In this case, however, we must consider the closed-loop constraint with transformation. If joint angles which do not fulfill the closed-loop constraint, internal force will be generated on each joint and this will damage the mechanics and electronics of the multirotor. Moreover, self-collision should be avoided for safe transformation.

We first use open-loop multilinks model, and then solve the inverse kinematics to satisfy the closed-loop constraint. Fig. 4 shows the kinematics model of the multilinks. If the

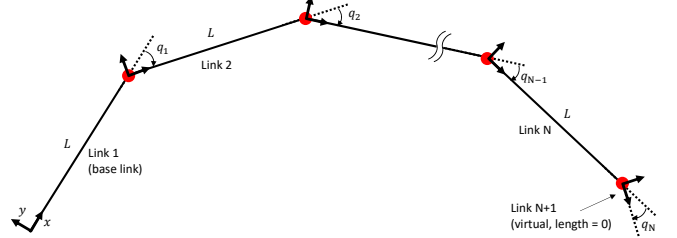


Fig. 4. Kinematics model of multilinks. The number of joints is n while the number of links is $n+1$. The length of the last link is 0, that is, the last link is a virtual link. Since it is not general that multilinks model ends with a joint, we define the virtual link whose length is 0. This configuration is for the joint angle constraint. We must consider all the joint angle limits because the real multilinks have closed-loop structure.

number of joints is N , the number of links is $(N+1)$. The length of the last link is 0, that is, the last link is a virtual link. Since it is not general that multilinks model ends with a joint, we define the virtual link whose length is 0. The reason of this configuration of the model is for joint angle constraint described latter. The coordinate of the $(N+1)$ th link is the coordinate of the end effector.

We design the transformation problem as Eq. 10.

$$\min_{\delta q} \|\delta q - \delta q_{ref}\|^2 \quad (10)$$

where δq and δq_{ref} are the infinitesimal joint angles and the error between the desired joint angles q_{ref} and current joint angles q , respectively.

Then, we add four constraints to Eq. 10 to generate interpolated forms which satisfy kinematics conditions.

A. Closed-loop Constraint

Given that δx is the error between the desired pose (comprising position and orientation) and current pose of the end effector, δq can be obtained with SR(singularity robust)-inverse[19] by solving Eq. 11.

$$\min_{\delta q} [(\mathbf{J}\delta q - \delta x)^T \mathbf{W}_1 (\mathbf{J}\delta q - \delta x) + \delta q^T \mathbf{W}_2 \delta q] \quad (11)$$

where \mathbf{J} is the jacobian of end effector. \mathbf{W}_1 and \mathbf{W}_2 are positive definite diagonal weight matrices. The SR-inverse is efficient to derive feasible joint angular velocities. In other words, we can reduce the effect of singularity by SR-inverse.

As already mentioned, in this paper our robot has closed-loop multilinks structure. The closed-loop constraint is simple: the pose of the origin of base link(1st link) coincides with the pose of end effector. In this case, since we configure the virtual last link, we address the coincidence of not positions but poses. Therefore, we set δx as follows:

$$\delta x = x_{base} - x_{end} \quad (12)$$

where x_{base} and x_{end} are the pose of the origin of base link and the pose of end effector, respectively.



Fig. 5. Joint angle limit with velocity damper method.

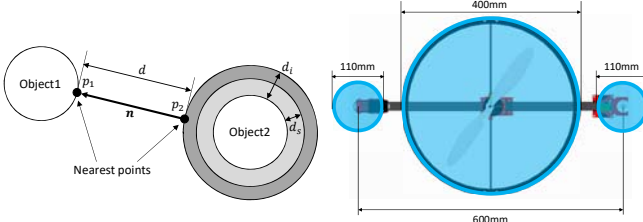


Fig. 6. Collision avoidance with velocity damper method.

Fig. 7. Geometric model for collision avoidance. Blue circles are given as the geometric model.

B. Joint Angle Constraint

In this work, the rotation range of each joint is $-\frac{\pi}{2} \sim \frac{\pi}{2}$ rad. The joint angles must be changed in this range. Then we use velocity damper[20] to set an inequality constraint. This is written as

$$\delta q_j^{min} \leq \delta q_j \leq \delta q_j^{max}, \text{ for } j \in \{1, \dots, n\} \quad (13)$$

$$\delta q_j^{min}(q_j) = \begin{cases} \delta q_j^{-} \frac{(q_j - q_j^{-}) - q_s}{q_i - q_s} & \text{if } q_j - q_j^{-} \leq q_i \\ \delta q_j^{-} & \text{otherwise} \end{cases} \quad (14)$$

$$\delta q_j^{max}(q_j) = \begin{cases} \delta q_j^{+} \frac{(q_j^{+} - q_j) - q_s}{q_i - q_s} & \text{if } q_j^{+} - q_j \leq q_i \\ \delta q_j^{+} & \text{otherwise} \end{cases} \quad (15)$$

where q_j^- and q_j^+ are the lower and upper limit of the joint angle and δq_j^- and δq_j^+ are the lower and upper limit of the infinitesimal change of the joint angle, respectively. q_i and q_s indicate the size of region where the joint angle is restricted and where the joint angle can not enter, respectively(Fig. 5). Normally, q_s is set to 0 in order to enable q_j to take the whole range.

C. Self-collision avoidance

We use the velocity damper again to set self-collision avoidance constraint. The constraint can be written as

$$\delta d \geq -\xi_d \frac{d - d_s}{d_i - d_s} \quad \text{if } d < d_i \quad (16)$$

where d is the shortest distance between two objects, ξ_d is the damping gain parameter, d_i is the threshold where the velocity damper works and d_s is the minimum distance secured between two objects (please refer Fig. 6). Given that p_1 and p_2 are the nearest points on the objects and n is the unit vector connecting p_2 to p_1 , δd can be written as

$$\delta d = \mathbf{n}(\mathbf{J}_{p_1} - \mathbf{J}_{p_2})\delta \mathbf{q} \quad (17)$$

where \mathbf{J}_{p_1} and \mathbf{J}_{p_2} are the jacobian of p_1 and p_2 , respectively.

To operate self-collision avoidance, robot geometric model must be set. Generally robots have complex shape and it is not easy to calculate distance between links of robots. Furthermore, to obtain continuous solution by this constraint, the objects are required to be strictly convex. Therefore, as shown in Fig. 7, we set the geometric model by approximation with circles. We must consider Eq. 16 on all pairs of circles, but because of the joint angle limitation, a link(i th) can not collide with the next($(i-1)$ th and $(i+1)$ th), and the next to the next($(i-2)$ th and $(i+2)$ th), resulting in a reduction of the calculation cost.

D. Singularity avoidance

As mentioned in Sec. II-B, \mathbf{Q} depends on the form \mathbf{q} , and the matrix \mathbf{Q} is not always full rank: we call this case ‘singular form’. If the form is singular, we can not obtain $\mathbf{Q}^\#$. Additionally, we can not obtain a practical solution by Eq. 9 if the form is close to a singular form. In this paper, we use the measure of manipulability [21] to evaluate the singularity. The measure of manipulability is defined as

$$w = \sqrt{\det(\mathbf{Q}\mathbf{Q}^T)} \quad (18)$$

Then, we apply the velocity damper again. The constraint is

$$\delta w = \frac{\partial w}{\partial \mathbf{q}} \delta \mathbf{q} \geq -\xi_w \frac{w - w_s}{w_i - w_s} \quad \text{if } w < w_i \quad (19)$$

where ξ_w is the damping gain parameter, w_i is the threshold where the velocity damper works and w_s is the minimum manipulability we want to keep.

To summarize, the transformation problem can be written as Eq. 20 and Eq. 21.

$$\begin{aligned} \min_{\delta \mathbf{q}} \quad & [\|\delta \mathbf{q} - \delta \mathbf{q}_{ref}\|^2 + (\mathbf{J}\delta \mathbf{q} - \delta \mathbf{x})^T \mathbf{W}_1 (\mathbf{J}\delta \mathbf{q} - \delta \mathbf{x}) \\ & + \delta \mathbf{q}^T \mathbf{W}_2 \delta \mathbf{q}] \\ \text{s.t.} \quad & \text{Eq. 13, Eq. 16, Eq. 19} \end{aligned} \quad (20)$$

$$\mathbf{q}_{k+1} = \mathbf{q}_k + \delta \mathbf{q} \quad (21)$$

Then, the weight matrices \mathbf{W}_1 and \mathbf{W}_2 must be designed properly. \mathbf{W}_1 indicates the weight of closed-loop constraint. As we use SR-inverse, there can be an error between the pose of the origin of base link and the pose of end effector, but the error is 0 on a real machine. Therefore, we set the diagonal elements of \mathbf{W}_1 as large values, and sufficiently small error can be absorbed by the impedance of servo motors. \mathbf{W}_2 indicates the penalty of change of joint angles. The larger the weight value is, the smaller the change of the joint angle is in an iteration.

We show the transformation by closed-loop multilinks with interpolation in Fig. 8. ① is the initial form and ⑨ is the target form, the input of the system. We set \mathbf{W}_1 to $\text{diag}(1.0 \times 10^6, \dots, 1.0 \times 10^6)$ and \mathbf{W}_2 to $\text{diag}(1.0 \times 10^6, \dots, 1.0 \times 10^6)$.

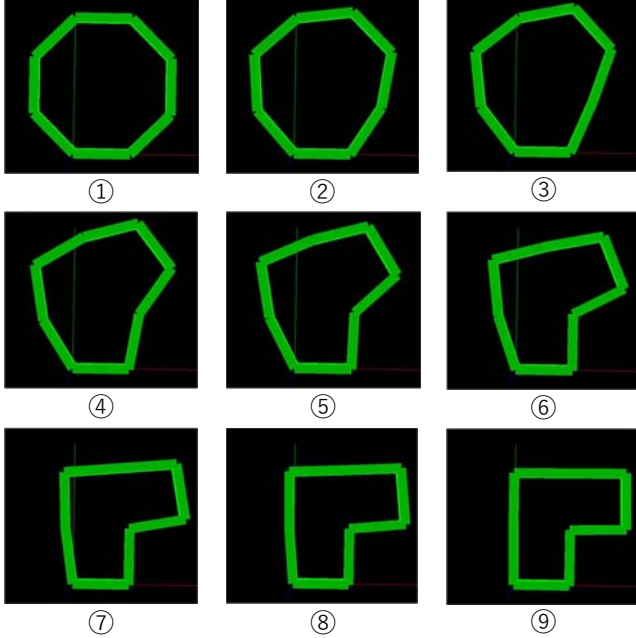


Fig. 8. Transformation with proposed interpolation method with closed-loop multilinks. ① is the initial form and ⑨ is the target form.

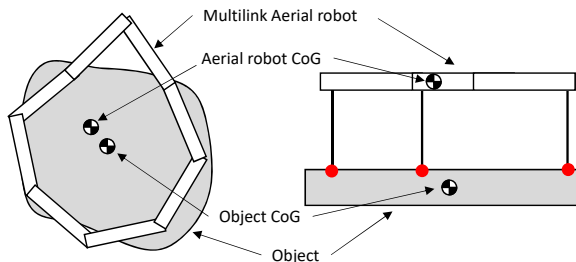


Fig. 9. Static model of object manipulation. The rigid flat object is hung with multiple grippers connected to the end of each cable. The red points indicate contact points.

$10^2, \dots, 1.0 \times 10^2$). As a result, interpolated forms satisfying the constraints can be obtained by the method.

IV. AERIAL GRASPING BASED ON SHAPE ADAPTIVE TRANSFORMATION

In this section, we explain a method to calculate a suitable form with regard to the shape of the target object. While there are several types of aerial grasping[1][6][12], we use multiple grippers connected to each cables for aerial grasping. Then, we address a problem of how to determine the pose and form of the multilinks based on static model.

A. Static Model of Object Grasping

As shown in Fig. 9, we consider the rigid flat object hung with grippers connected to the end of cable. To simplify the problem, we assume that each cable is vertical and the length is the same, that is the carried flat object is parallel to the aerial robot. Given that \mathbf{p}_{obj} is the object CoG position

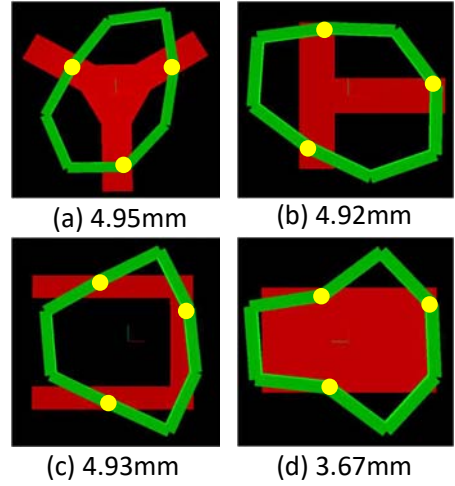


Fig. 10. Results of form calculation based on flight stability. The target objects are indicated with red. Yellow circles indicate the position of grippers. Each number below each case is the two-dimensional distance between aerial robot CoG and object CoG.

described in aerial robot CoG frame, the force \mathbf{f}_{obj} and torque $\boldsymbol{\tau}_{obj}$ produced by the object can be calculated as

$$\mathbf{f}_{obj} = M_{obj}\mathbf{g} \quad (22)$$

$$\boldsymbol{\tau}_{obj} = \mathbf{p}_{obj} \times \mathbf{f}_{obj} \quad (23)$$

where M_{obj} is the mass of the object. \mathbf{f}_{obj} and $\boldsymbol{\tau}_{obj}$ are disturbances to the flight control system of the aerial robot. As you know, \mathbf{f}_{obj} is constant regardless of \mathbf{p}_{obj} . On the other hand, $\boldsymbol{\tau}_{obj}$ changes by \mathbf{p}_{obj} .

B. Form Calculation Method based on Flight Stability

Here, we introduce virtual joint link of base link and use generalized jacobian[22]. Then, we modify \mathbf{q} with adding the joint angles of virtual joint link. This is written as

$$\tilde{\mathbf{q}} = [q_x \ q_y \ q_\varphi \ q_1 \ q_2 \ \dots \ q_n] \quad (24)$$

Note that we consider the pose of base link in two dimension with the assumption that the object is parallel to the aerial robot, and z is constant when the aerial robot grasps the object.

Then, we aim to minimize the disturbance torque $\boldsymbol{\tau}_{obj}$ for stable flight. Since $\boldsymbol{\tau}_{obj}$ equals to $\mathbf{0}$ when \mathbf{p}_{obj} is $\mathbf{0}$, we propose minimization of the norm of \mathbf{p}_{obj} . This problem can be rephrased to the problem that the aerial robot CoG coincides with the object CoG. Therefore, this problem can be solved as a general inverse kinematics problem. This is written as

$$\min_{\delta\tilde{\mathbf{q}}} (\mathbf{J}_{CoG}\delta\tilde{\mathbf{q}} - \delta\mathbf{x}_{CoG})^T \mathbf{W}_3 (\mathbf{J}_{CoG}\delta\tilde{\mathbf{q}} - \delta\mathbf{x}_{CoG}) \quad (25)$$

where \mathbf{J}_{CoG} is the jacobian of aerial robot CoG, \mathbf{x}_{CoG} is the error between the desired CoG position and current CoG position and \mathbf{W}_3 is a weight matrix. Then, similar to Sec. III,

we add constraints to obtain feasible solution. While closed-loop constraint (Sec. III-A), joint angle constraint (Sec. III-B), self-collision avoidance (Sec. III-C) and singularity avoidance (Sec. III-D) are also necessary, we add one more constraint that all cables must be attached to the target object. In other words, all contact points must overlap the object as viewed from above. This problem is similar to self-collision avoidance (Sec. III-C). There are two differences. First, we consider the contact point as a point, not an area (object1 in Fig. 6) and as the target object is fixed (object2 in Fig. 6) in the global coordinate system, \mathbf{J}_{p2} is \mathbf{O} . Thus, Eq. 17 can be rewritten as

$$\delta d = \mathbf{n} \mathbf{J}_{p1} \delta \tilde{\mathbf{q}} \quad (26)$$

Second, in Sec. III-C we start the calculation with a situation where the objects do not collide, so always the objects do not collide due to the velocity damper. However, here we must consider a situation where the contact point is both inside and outside the target object. Therefore, in this section Eq. 16 is redefined as

$$\delta d_j \geq \begin{cases} -\xi_d \frac{d - d_s}{d_i - d_s} & \text{if } d_s < d_j < d_i \\ \alpha & \text{if } d < d_s \\ -\infty (\text{no constraint}) & \text{otherwise} \end{cases} \quad (27)$$

Note that we define d as positive value if the point is inside the object and negative value if it is outside. α is small positive value by which the point moves into the object.

Combining all constraints, the form calculation problem can be written as Eq. 28 and Eq. 29.

$$\begin{aligned} \min_{\delta \tilde{\mathbf{q}}} \quad & [(J \delta \mathbf{q} - \delta \mathbf{x})^T \mathbf{W}_1 (J \delta \mathbf{q} - \delta \mathbf{x}) + \delta \tilde{\mathbf{q}}^T \mathbf{W}_2 \delta \tilde{\mathbf{q}} \\ & + (J_{CoG} \delta \tilde{\mathbf{q}} - \delta \mathbf{x}_{CoG})^T \mathbf{W}_3 (J_{CoG} \delta \tilde{\mathbf{q}} - \delta \mathbf{x}_{CoG})] \\ \text{s.t.} \quad & \text{Eq. 13, Eq. 16, Eq. 19, Eq. 27} \end{aligned} \quad (28)$$

$$\tilde{\mathbf{q}}_{k+1} = \tilde{\mathbf{q}}_k + \delta \tilde{\mathbf{q}} \quad (29)$$

Then, we calculate optimized forms by Eq. 28 and Eq. 29 as shown in Fig. 10. Yellow circles indicate the position of contact points and they are successfully bound on the object by the constraint. Each number below each case is the two-dimensional distance between aerial robot CoG and object CoG. In this work, we stop the calculation at the moment the two-dimensional distance becomes lower than 5 mm, as fully converged. Since the calculation is converged on all the case, it is concluded that suitable forms can be obtained by this method.

V. EXPERIMENTS

A. Aerial Transformation

We performed an experiment of aerial transformation by the octorotor with close-loop structure with our proposed method described in Sec. III. As shown in Fig. 11, we set four key forms. The initial form ① and the last form ④ are the same. Eq. 20 was solved and the joint angles were updated

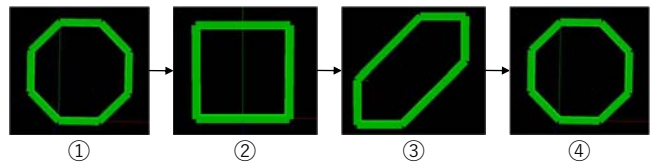


Fig. 11. Key forms for the experiment of aerial transformation. The initial form ① and the last form ④ are the same.

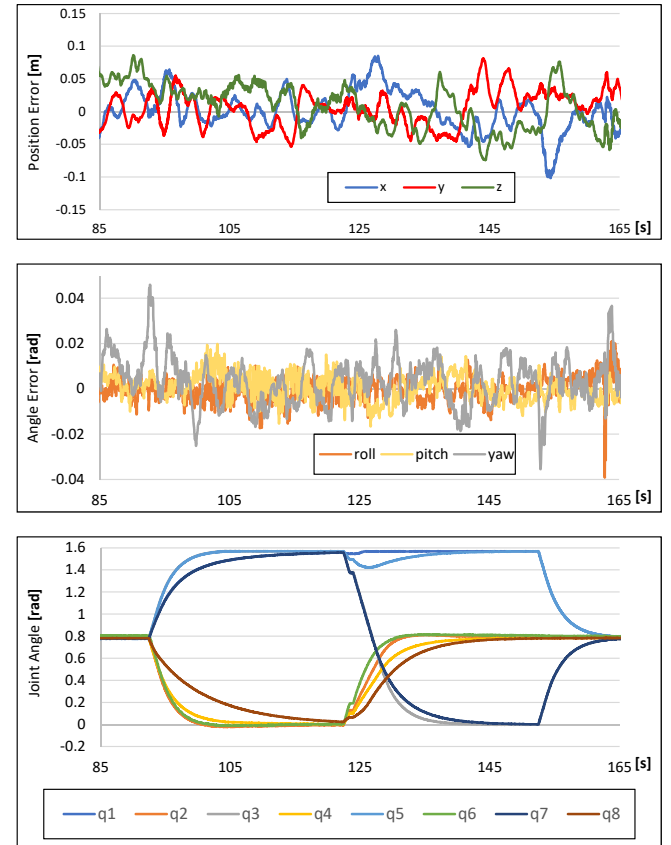


Fig. 12. The result of aerial transformation. Upper: change of three-dimensional position error(x, y, z). Middle: change of attitude angles error(roll, pitch and yaw). Lower: change of each joint angle.

at 20 Hz. The weight parameters were the same as the ones of Sec. III. The three-dimensional position was tracked by a motion capture system. The result of the experiment is shown in Fig. 12. The joint angles changed to the target angles correctly and transformation was fully performed. The problems which occurred due to low rigidity was solved by closed-loop structure. Moreover, in spite of the large inertia, the trackability of x, y and yaw angle is improved due to the fully-actuated control. While in our previous transformation experiment[13], the maximum position error was about 0.3 m, it is about 0.1 m in this experiment. Then we conclude that the feasibility of the aerial transformation and the effectiveness of the fully-actuated control by the octorotor with closed-loop structure was experimentally demonstrated.

B. Aerial Shape Adaptive Grasping

In this experiment, the transformable aerial robot grasps a large object and hovers in the air. The shape of the target object was Fig. 10(a) and its surface was ferrous to be able to absorb by magnet grippers. The weight of the object was 1.25 kg. The form was calculated with form calculation method described in Sec. IV. Fig. 1 is a snapshot of this experiment. The object was hung with magnet grippers connecting to the aerial robot. Then we show the experimental result in Fig. 13. Compared with the previous experiment(Sec. V-A), the convergence of position and attitude is lower, but the multirotor could keep stable hovering. Note that the altitude z did not reach to the target value with a stationary error. That is because, we consider, the wind produced by each propeller hit to the object and down force was generated. We therefore conclude that the effectiveness of the form calculation method was shown and we also conclude that the aerial grasping by HALO was achieved.

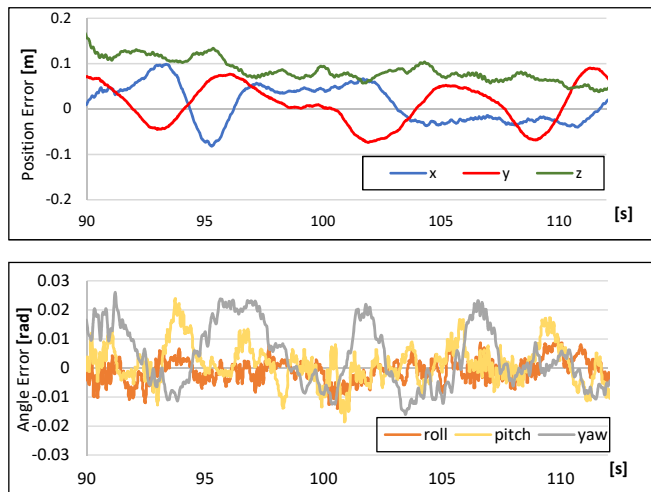


Fig. 13. The result of hovering with the large object. Upper: change of three-dimensional position error(x, y, z). Lower: change of attitude angles error(roll, pitch and yaw).

VI. CONCLUSIONS

In this paper, we proposed the multirotor with two-dimensional closed-loop multilinks for large and various shapes of object grasping. We constructed the new link module with the tilted propeller and introduced fully-actuated flight control system. We then developed the transformation method for closed-loop multilinks by which interpolated forms can be obtained. We also described form calculation method for shape adaptive 2D transformation. By this method, the disturbance torque produced by the target object is minimized for stable hovering. Finally, we showed the effectiveness of our proposed methods by experimental results of aerial transformation and aerial grasping based on shape adaptive 2D transformation.

For future work, while in this work we addressed only object grasping, we will try aerial manipulation with consideration of the dynamics between the object and the multirotor.

Furthermore, the octo type HALO has the singularity form problem. In our previous works[11][13], the two-dimensional transformable multirotor had also the same problem. If we solve this problem by a mechanical modification, the range of application spreads widely.

REFERENCES

- [1] D. Mellinger *et al.* Design, modeling, estimation and control for aerial grasping and manipulation. In *IROS 2011*, pp. 2668–2673, 2011.
- [2] M. Bernard and K. Kondak. Generic slung load transportation system using small size helicopters. In *ICRA 2009*, pp. 3258–3264, 2009.
- [3] F. Huber *et al.* First analysis and experiments in aerial manipulation using fully actuated redundant robot arm. In *IROS 2013*, pp. 3452–3457, Nov 2013.
- [4] Matko Orsag, Christopher Korpela, and Paul Oh. Modeling and control of mm-uav: Mobile manipulating unmanned aerial vehicle. *Journal of Intelligent & Robotic Systems*, Vol. 69, No. 1, pp. 227–240, Jan 2013.
- [5] D. R. McArthur, A. B. Chowdhury, and D. J. Cappelleri. Design of the i-boomcopter uav for environmental interaction. In *ICRA 2017*, pp. 5209–5214, May 2017.
- [6] Jonathan Fink *et al.* Planning and control for cooperative manipulation and transportation with aerial robots. *The International Journal of Robotics Research*, Vol. 30, No. 3, pp. 324–334, 2011.
- [7] Michael Gassner, Titus Cieslewski, and Davide Scaramuzza. Dynamic collaboration without communication: Vision-based cable-suspended load transport with two quadrotors. In *ICRA 2017*, 2017.
- [8] Hyoin Kim *et al.* Motion planning with movement primitives for cooperative aerial transportation in obstacle environment. In *ICRA 2017*, 2017.
- [9] M. Manubens, D. Devaurs, L. Ros, and J. Cortes. Motion planning for 6-d manipulation with aerial towed-cable systems. In *Robotics: Science and Systems*, June 2013.
- [10] V. Lippiello *et al.* Hybrid visual servoing with hierarchical task composition for aerial manipulation. *IEEE Robotics and Automation Letters*, Vol. 1, No. 1, pp. 259–266, Jan 2016.
- [11] Moju Zhao *et al.* Transformable multirotor with two-dimensional multilinks: modeling, control, and motion planning for aerial transformation. *Advanced Robotics*, Vol. 30, No. 13, pp. 825–845, 2016.
- [12] Moju Zhao *et al.* Whole-body aerial manipulation by transformable multirotor with two-dimensional multilinks. In *ICRA 2017*, 2017.
- [13] Tomoki Anzai *et al.* Multilinked multirotor with internal communication system for multiple objects transportation based on form optimization method. In *IROS 2017*, 2017.
- [14] S. Park, J. Her, J. Kim, and D. Lee. Design, modeling and control of omni-directional aerial robot. In *IROS 2016*, pp. 1570–1575, Oct 2016.
- [15] R. Voyles and G. Jiang. Hexrotor uav platform enabling dexterous interaction with structures - preliminary work. In *2012 IEEE International Symposium on Safety, Security, and Rescue Robotics (SSRR)*, pp. 1–7, Nov 2012.
- [16] M. Ryll, D. Bicego, and A. Franchi. Modeling and control of fast-hex: A fully-actuated by synchronized-tilting hexarotor. In *IROS 2016*, pp. 1689–1694, Oct 2016.
- [17] Yuji Tsusaka, Yakeshi Fukuzumi, and Hirochika Inoue. Parallel manipulator: Its design and mechanical characteristics. *Journal of the Robotics Society of Japan*, Vol. 5, No. 3, pp. 180–188, 1987.
- [18] Feng Gao *et al.* New kinematic structures for 2-, 3-, 4-, and 5-dof parallel manipulator designs. *Mechanism and Machine Theory*, Vol. 37, No. 11, pp. 1395 – 1411, 2002.
- [19] Yoshihiko NAKAMURA and Hideo HANAFUSA. Singularity low-sensitive motion resolution of articulated robot arms. *Transactions of the Society of Instrument and Control Engineers*, Vol. 20, No. 5, pp. 453–459, 1984.
- [20] Fumio Kanehiro *et al.* Reactive leg motion generation method under consideration of physical constraints. *Journal of the Robotics Society of Japan*, Vol. 28, No. 10, pp. 1251–1261, 2010.
- [21] Tsuneo Yoshikawa. Manipulability of robotic mechanisms. *The International Journal of Robotics Research*, Vol. 4, No. 2, pp. 3–9, 1985.
- [22] Yoji UMETANI and Kazuya YOSHIDA. Resolved motion rate control of space robotic manipulators with generalized jacobian matrix. *Journal of the Robotics Society of Japan*, Vol. 7, No. 4, pp. 327–337, 1989.